Superconductive quantum size effect in indium films

F. E. Vopat,* T. S. A. Lai,† and W. J. Tomasch
Department of Physics, University of Notre Dame, Notre Dame, Indiana 46556
(Received 15 October 1985; revised manuscript received 15 September 1986)

Thick In films ($d_S = 5$–41 μm), backed by thinner Al (≈ 0.2 μm) to yield In/Al bilayers, are incorporated into Al—Al-oxide—In/Al tunnel junctions. Because of Andreev reflections at the In-Al interface, first-derivative tunneling spectra (dV/dI) contain virtual-state levels (oscillations) whose spacings scale as $1/d_S$. Amplitudes and spacings depend directly on the electron-phonon renormalization, $Z_S(E)$, of In. Our In films are characterized by strong [001] and [111] crystalline fiber textures that coexist. Most In films ($\approx 75\%$) produce simple spectra characterized by a single dressed velocity $v_{FS}^* = (1.151 \pm 0.007) \times 10^6 m/s$. The remainder produce beat-modulated spectra characterized by just two velocities, $v_{FS1}^* = (1.166 \pm 0.014) \times 10^6$ and $v_{FS2}^* = (1.062 \pm 0.015) \times 10^6 m/s$. We attribute beats to coexisting textures and consequent tunneling from two patches of the Fermi surface. Inferred mass enhancements, $\lambda = 1 - Z_S(0) = 0.49$ and 0.62, are appropriate for second-zone holes. All In films yield similar energy-gap values. Their average (0.53 ± 0.01 meV) corresponds to a nominal BCS coherence length of 0.23 μm. An anomalous shoulder occurs in the dV/dI background, just above the main gap edge. If attributed to third-zone electron tunneling, this shoulder would correspond to an average gap of (0.65 ± 0.05) meV. We infer $\mathrm{Re}Z_S(E)/Z_S(0)$ by requiring a theoretical spectrum to reproduce the observed bias locations of peaks and dips in dV/dI, i.e., to reproduce the observed energy levels. These results are similar to those obtained from Rowell-McMillan tunneling spectroscopy, although our $Z_S(0)$ values are significantly smaller. We also attempt to infer $\mathrm{Im}Z_S(E)$ by fitting dV/dI oscillation amplitudes. This task is complicated by the invariable occurrence of anomalously strong level amplitudes at lower biases ($V < 1.0$ mV). Whereas the energy-level locations are quite reasonable, we are unable to provide a compelling explanation of the dV/dI amplitudes. Possible alternatives, including gap enhancement, are mentioned. Amplitude and background anomalies occupy the same bias range and always occur together. They occur whenever overall amplitudes are sufficiently strong, and are probably characteristic of pure, single-crystal In.

I. INTRODUCTION

The spatially localized gap perturbation associated with a superconducting-normal (S/N) interface [$\Delta_S(\mathrm{In}) > \Delta_N(\mathrm{Al})$] causes Andreev scattering[1] that crosslinks electronlike ($k > k_F$) and holelike ($k < k_F$) components of an excitation. Interference between an incoming quasiparticle (in S) and its reflection produces standing waves in a clean, uniform S layer (backed by N). Resulting virtual-state structure in the charge-carrier density of states comprises a superconducting quantum size effect (SQSE).[2–12] Corresponding SQSE levels are observed in S-side tunneling spectra. (Plots of dV/dI and d^2V/dI^2 versus V are referred to as first-derivative and second-derivative SQSE spectra.) For "dirty" overlayers (Wolfram limit) and energies above $E \approx 2\Delta_S$, theory[6,11] predicts level spacings and amplitudes that approach $[hv_{FS}^*/4d_S][Z_S(0)/\mathrm{Re}Z_S(E)]$ and $\exp[-\gamma_S \mathrm{Im}Z_S(E)E]$, respectively. Film thickness (d_S), mean free path (l_S), and dressed Fermi velocity (v_{FS}^*) determine $C_S = 4d_S/hv_{FS}^*$ and $\gamma_S = 2d_S/l_S$. Levels are finally quenched by spontaneous phonon emission (SPE) at a characteristic energy ($E_S \approx 3.5$ meV for In). At low energies ($E < 2\Delta_S$), $\Delta_S(E)$ and $Z_S(E)$ can both influence spectra, but at higher energies, $Z_S(E)$ tends to dominate.

Because theoretical spectra[6,11,12] depend on $Z_S(E)$ explicitly, comparisons with experiment permit $\mathrm{Re}Z_S(E)/Z_S(0)$ and $\mathrm{Im}Z_S(E)$ to be inferred ($eV < E_S$). These comparisons are implemented by assuming that $\Delta_S(E)$ and $Z_S(E)$ are well behaved and slowly varying at low energies. Inversion of the appropriate Eliashberg equation then yields the weighted phonon spectrum, $\alpha^2F(\omega)$.

On the other hand, our experiment measures dressed Fermi velocities, v_{FS}^*, directly, without assumptions regarding $\Delta_S(E)$ or $Z_S(E)$. Combining v_{FS}^* with theoretical estimates of the bare Fermi velocity, v_{FS} [$= Z_S(0)v_{FS}^*$], yields a hybrid determination of the mass enhancement, $\lambda = [Z_S(0) - 1]$.

Although we obtain reasonable results for v_{FS}^*, λ, and $\mathrm{Re}Z_S(E)/Z_S(0)$, our results for $\mathrm{Im}Z_S$ ($E < 3.0$ meV) contain unexpected structure directly attributable to unusually strong level amplitudes at lower biases ($V < 1.0$ mV). Experimental amplitudes just above the sum-of-gaps signature (SGS: $V \approx 0.7$ mV) consistently exceed those predicted by extrapolations from higher biases. This is the low-bias amplitude anomaly (LBAA). It influences the fitting process via γ_S and introduces structure in $\mathrm{Im}Z_S(E)$ that may well be artificial.

Dynamic-resistance (dV/dI) backgrounds, constructed empirically to produce symmetrical peak and dip amplitudes, also exhibit an anomalous shoulder just above the

main gap edge. This is the dynamic-resistance background anomaly (DRBA).

The two anomalies occupy approximately the same bias range, $0.75 \leq V \leq 0.9$ mV at $T=0.3$ K. Experience suggests that the two occur whenever SQSE amplitudes are reasonably strong. We have never observed the one without the other. Because our In films exhibit pronounced crystalline fiber textures and very large mean-free-path values, this behavior may well be characteristic of pure, single-crystal In.

II. AN OVERVIEW OF EXPERIMENTAL RESULTS

A. Junctions, fiber textures, and solitary crystallites

1. Junction fabrication

All metal films are evaporated at ambient pressures in the range 5×10^{-8}–5×10^{-7} Torr. Aluminum counterelectrodes [CE: $\approx$0.5 mm $\times$ 10 mm $\times$(0.03–0.3) μm] on glass are exposed to room air to form Al oxide tunnel barriers. Perpendicular films of very thick In (5–41 μm) then yield four-terminal tunnel junctions. Finally, the exposed In is promptly overlayed with thin Al ($d_N \approx 0.2$ μm). Indium film thicknesses are determined by Michelson interferometry.

Figure 1 presents an $I(V)$ trace for a junction (In thickness $d_S = 34.7$ μm) with typically good barrier properties. The absence of leakage current at low biases shows that charge transfer is by tunneling. Junctions frequently retain their low-leakage properties after prolonged vacuum storage (annealing) at room temperature.

The cusp ($V \approx 0.3$ mV at 0.6 K) and the rapid current increase ($V \approx 0.7$ mV at 0.3 K) occur at $eV = \Delta_S - \Delta_{CE}$ and $eV = \Delta_S + \Delta_{CE}$, respectively. The latter causes the pronounced dip in dV/dI that defines the SGS.

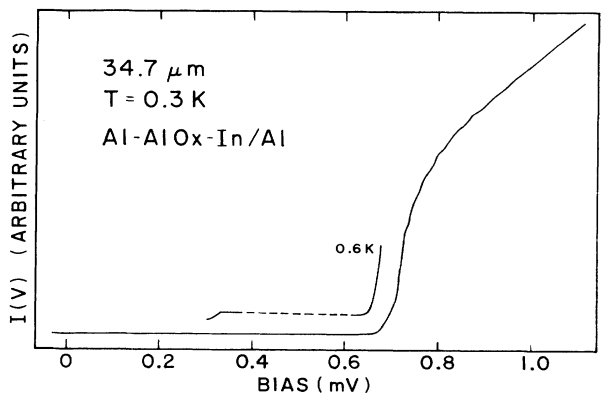

FIG. 1. A representative current-voltage characteristic, $I(V)$, obtained with an In film 34.7 μm thick. SQSE levels are sufficiently strong to produce ripples in $I(V)$ just above the sum-of-gaps signature (SGS: $V \approx 0.7$ mV).

2. Binary fiber textures and solitary crystallites

X-ray diffractometer studies of thick In surrogate films yield strong [001] and [111] textures that coexist. Surrogates are deposited on glass or on glass-Al-Al oxide by the same methods employed for fabricating junctions. Although [001] tends to dominate, the coexisting [111] can rival its strength. Together, they account for all observed x-ray lines, there being no powder pattern component. If substrates are warmed during deposition ($\approx$90 °C), a pure [111] texture results. This suggests metastable retention of the majority [001] texture.

Visual examinations (10–100$\times$) of our In films reveal a finegrained background, in which larger, solitary crystallites [$\approx$(0.1–0.3)-mm diameter] are embedded. These appear dark and glossy, and are visually absent from warmed surrogates ($\approx$90 °C), i.e., from films with pure [111] textures. Consequently, these larger crystallites may comprise a metastable [001] texture.

B. Virtual-state level structure

1. Introduction

Of 19 Al-Al oxide-In/Al junctions, two produce weak spectra and seventeen produce either strong or very strong spectra. As indicated in Fig. 1, level structure just above the SGS ($V \approx 0.7$ mV) can be sufficiently strong to be seen directly as ripples in $I(V)$. Figure 2 presents a high-quality, calibrated dV/dI spectrum acquired with a sister diode, i.e., one produced during the same fabrication cycle. This data set will later be used to infer the real and imaginary parts of $Z_S(E)$. The second-derivative spectrum produced by a third sister appears in Figs. 3 and 4. All three sisters show comparably strong effects, and to a good precision, all yield the same Fermi velocity. Good

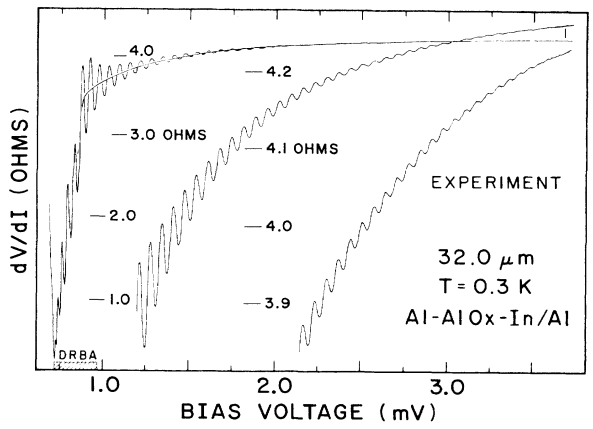

FIG. 2. A very strong, simple dV/dI spectrum produced by an In film 32.0 μm thick. Level amplitudes below 1.0 mV are substantially larger than anticipated from higher-bias extrapolations. These larger amplitudes ($V < 1.0$ mV) comprise the low-bias amplitude anomaly (LBAA). DRBA stands for dynamic resistance (dV/dI) background anomaly—a bulge in the background that becomes conspicuous on a finer voltage scale (Fig. 9). The LBAA and DRBA occupy the same bias range (shaded area).

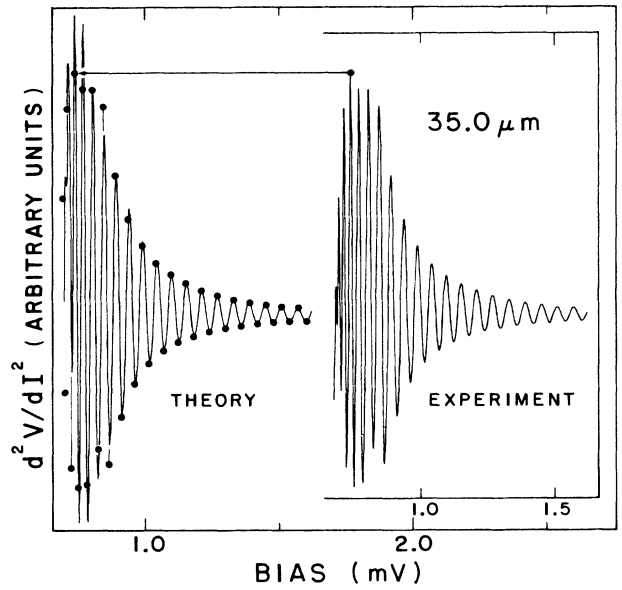

FIG. 3. Low-bias portion of a very strong, simple d^2V/dI^2 spectrum ($T=0.9$ K). The corresponding dV/dI spectrum (not shown) exhibits a well-developed LBAA. Dots locate experimental peaks and dips for later comparisons with theory. Below 0.9 mV, computed amplitudes exceed observed amplitudes because of the $\mathrm{Im}Z_S(E)$ variation employed [Fig. 17, curve (a)]. A more conventional variation [Fig. 17, curve (b)] seriously underestimates experimental amplitudes in the DRBA/LBAA range. Computed spectra take temperature, nonspecular tunneling ($\beta\approx 15°$), and gap broadening [$\mathrm{Im}\Delta(0)/\mathrm{Re}\Delta(0)=1\%-3\%$] into account.

internal consistency is maintained when comparisons are extended to independently fabricated junctions that may exhibit somewhat weaker effects. At higher biases, amplitudes depicted in Figs. 2–4 decay monotonically with increasing bias. This is the defining property of a *simple* spectrum.

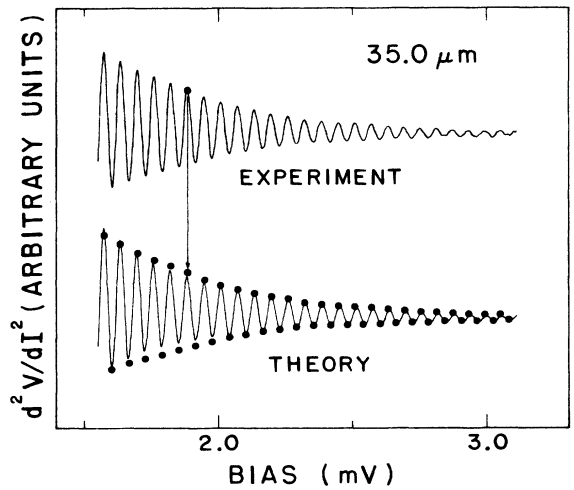

FIG. 4. High-bias portion of preceding spectrum (Fig. 3).

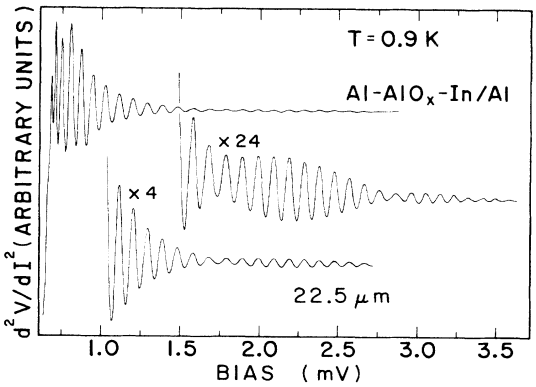

FIG. 5. A strong, beat modulated d^2V/dI^2 spectrum. Three beats occur over the full bias range. The last beat is terminated prematurely by spontaneous phonon emission (SPE).

2. *Simple and beat-modulated spectra*

Fourteen of nineteen junctions produce simple derivative spectra like those already shown, except that overall amplitudes are often somewhat weaker. At higher biases, these majority spectra resemble those predicted for tunneling from a single patch of the Fermi surface.[6,11] At biases above 3.6 mV (corresponding to $E_S\approx 3.5$ meV), all level structure is quenched by SPE, i.e., by a rapid increase in $\mathrm{Im}Z_S(E)$. Quenching near 3.6 mV is a property shared by all junctions.

The five minority junctions produce beat modulated spectra such as those presented in Figs. 5–7. The general appearance of these spectra suggests interference between

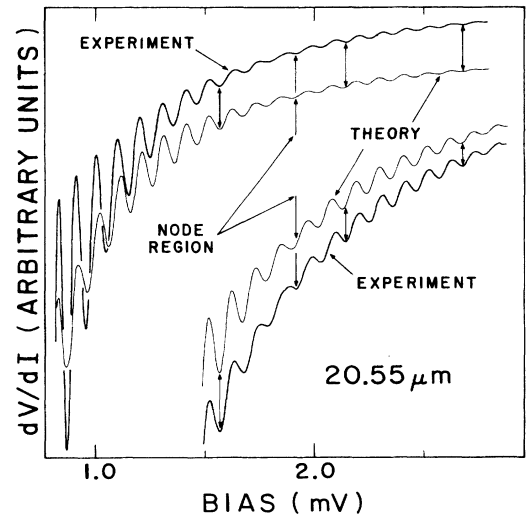

FIG. 6. A very strong, beat modulated dV/dI spectrum ($T=0.9$ K). Reference arrows locate experimental dips. The computed spectrum is a single-gap, two-velocity (SGTV) result in which two sets of levels are added in the ratio 2:1. Use of a conventional $\mathrm{Im}Z_S(E)$ variation [similar to Fig. 17, curve (b)] seriously underestimates low-bias amplitudes as shown. This is the hallmark of the LBAA.

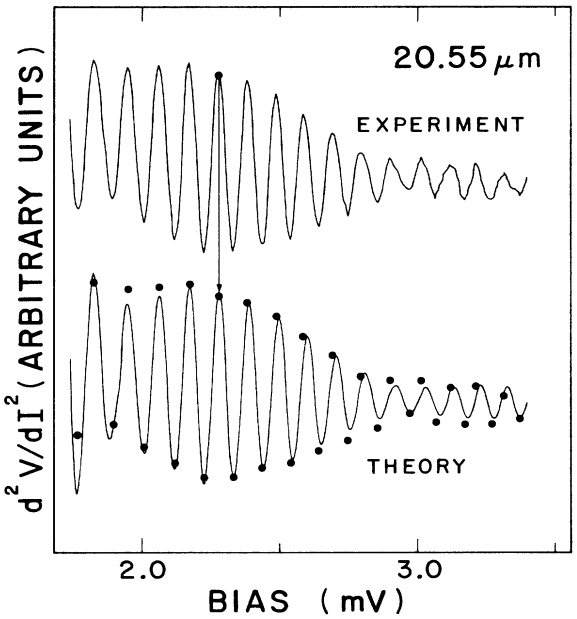

FIG. 7. High-bias portion of the d^2V/dI^2 spectrum for the junction of Fig. 6. Dots locate experimental peaks and dips. A computed SGTV spectrum is also plotted.

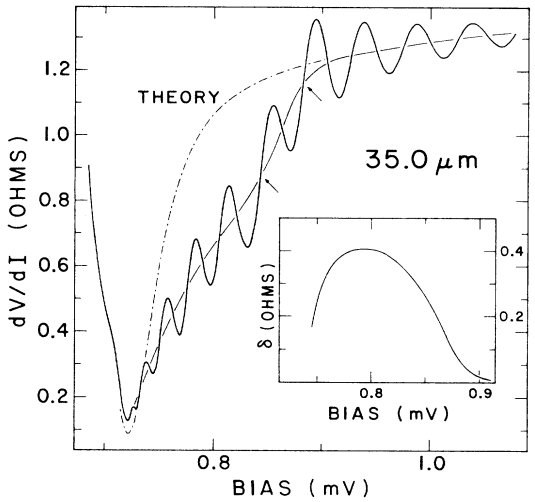

FIG. 8. Low-bias portion of a strong, simple spectrum ($T=0.3$ K). An empirical background (nonoscillatory solid curve) yields symmetrical ($\pm$) oscillations. Its shoulder defines the DRBA. A strong-coupling BCS background (broken curve) is also plotted, and the inset gives the difference between backgrounds—the anomalous excess. Arrows indicate level distortions characteristic of the steep portion of the DRBA.

two simple spectra that differ in period by about 10%. All five junctions produce strong or very strong amplitudes.

3. *The DRBA*

Both simple and beat-modulated spectra seem to exhibit background anomalies when level amplitudes are sufficiently strong. Figure 8 presents a clear example of this behavior for the strong, simple spectrum produced by the junction of Figs. 3 and 4.[13] This junction also exhibits a well-developed LBAA in dV/dI. The DRBA shoulder is approximately 0.2 mV wide and lies about 0.1 mV above the SGS. Complex spectra, described in the following section, also afford good examples of the DRBA.

4. *Complex spectra*

Only two of the 19 junctions yielded complex spectra at some point in their history. Both produced complex spectra after prolonged (1—2 year) room-temperature annealing in a rough vacuum.

The first junction produces a simple preanneal spectrum (not shown) that yields the appropriate value of $v_{FS}^*(0)$. Its complex postanneal spectrum (not shown) is characterized by the reoccurrence of short wavelengths in the DRBA bias range. (This is also true for the postanneal spectrum of the second junction, described below.) Complexities are confined to the DRBA/LBAA range. A standard, reasonably strong, beat modulated spectrum is observed at higher biases ($V \geq 1.0$) after annealing.

The second junction yields a preanneal dV/dI spectrum (not shown) that evidences weak additional level structure ($0.7 \leq V \leq 0.8$ mV) and lineshape asymmetries ($0.8 \leq V \leq 1.1$ mV) in the first six oscillations. Overall effects resemble those of interference between a strong main series and a much weaker second series. Prior to annealing, this junction produces a standard beat modulated spectrum (Fig. 5) at higher biases.

Figure 9 presents the low-bias portion of the corresponding postanneal dV/dI spectrum, which exhibits reduced overall amplitudes and pronounced complexity at lower biases ($V \leq 1.2$ mV). The first two levels appear normal and *strong*, but the third fails to materialize. Instead, the DRBA background now supports short-wavelength structure—as if a new series were being initiated ($V=0.77$—0.80 mV). Subsequent structure is weaker and more complex than anticipated from the first two levels. This behavior is qualitatively consistent with destructive interference between *strong* series. At higher biases ($V > 1.5$ mV), this junction continues to produce a beat modulated spectrum, but with amplitudes substantially weaker than those obtained before annealing.

Annealing seems to yield complex spectra only occasionally. The strong simple spectrum of Fig. 2, for example, was obtained after a comparably long anneal. This suggests that reductions in amplitude produced by long-term annealing are not due to reductions in the mean free path, but rather to destructive interference between *strong* series.

Initiation of a new series might be expected to require a new gap signature, i.e., an additional dip in dV/dI. This could account for the pronounced DRBA (shoulder) of Fig. 9. If reduced level amplitudes result from destructive interference between strong series, rather than (say) from a decreased mean free path, such amplitude reductions should help emphasize the DRBA. Together, these two

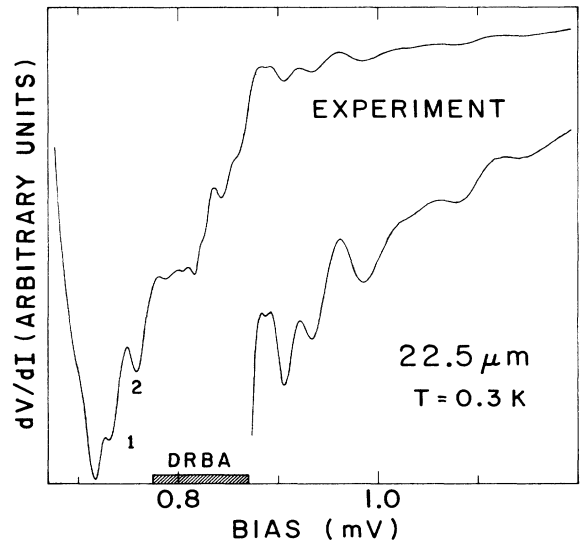

FIG. 9. Complex postanneal spectrum produced by the junction of Fig. 5. Overall junction quality remains good (low leakage), but level structure has weakened and become complicated. The first two levels (labeled) are simple and quite strong, suggesting that subsequent structure is weak because of destructive interference between several *strong* series. This is the strongest DRBA we have observed.

considerations may explain why the DRBA in Fig. 9 is the most prominent we have ever observed.

5. *The LBAA*

Perusal of Fig. 2 suggests that dV/dI amplitudes at lower biases ($V \leq 1.0$ mV) are large compared to those one might anticipate from amplitudes at higher biases. Put differently, the survival of high-bias structure (1.5—3.6 mV) seems surprising in view of the rapid decrease in amplitudes near 1.0 mV. The same is true for beat modulated spectra. This general trend becomes quite clear during quantitative comparisons of dV/dI with theory. If a conventional $\mathrm{Im}Z_S(E)$ variation is utilized, computed amplitudes are much smaller than those observed, as in Fig. 6 ($V < 1.2$ mV). A more complicated $\mathrm{Im}Z_S(E)$ can improve this situation in an average way that overestimates amplitudes of the lowest-lying levels, as in Fig. 3.

III. COMPARISON OF EXPERIMENT AND THEORY

A. Introduction

1. *Goals*

Ultimately, SQSE spectroscopy hopes to infer v_{FS}^*, λ, $\mathrm{Re}Z_S$ ($E \leq E_S$)$/Z_S(0)$, $\mathrm{Im}Z_S$ ($E \leq E_S$), and α^2F ($\omega \leq \omega_S$), and to associate these with tunneling from specific patches of the Fermi surface. But analyses of SQSE spectra are straightforward only for single-patch tunneling, and even a single In orientation may contribute multiple patches because of Fermi-surface complexity. Binary textures, beat-modulated spectra, and low-bias anomalies portend interpretive difficulties. Nevertheless, the first three goals appear attainable, and at least some progress is possible for the other two ($E > 3.0$ meV).

2. *Interpretation of simple and beat modulated spectra*

We will find that, to good precision, all simple spectra yield the same numerical Fermi velocity (v_{FS}^*). This strongly suggests that all simple spectra are due to tunneling from a single, unique patch of the Fermi surface. We will infer $\mathrm{Re}Z_S(E)/Z_S(0)$ by computer fitting a single-series theoretical spectrum to the observed energy levels of a representative dV/dI spectrum (Fig. 2). This will prove successful in that a reasonable variation of $\mathrm{Re}Z_S(E)/Z_S(0)$ provides good agreement at all energies. An analogous procedure for utilizing $\mathrm{Im}Z_S(E)$ to fit amplitudes produces only fair agreement in the DRBA/LBAA range. Furthermore, fitting amplitudes in the DRBA/LBAA range with existing theory requires an unusual $\mathrm{Im}Z_S(E)$ variation. Aside from these amplitude difficulties, however, treating simple spectra in terms of tunneling from a single patch meets with considerable success.

A natural extension of the above view attributes beat modulated spectra to tunneling from two patches on the Fermi surface. Gallagher compound resonances[12] could, however, provide an alternative explanation, since under appropriate conditions, these resonances exhibit beats very similar to those observed. We will show that compound resonances do not provide a quantitatively successful description of modulation envelopes, whereas two-patch tunneling does.

Fermi-surface geometry and crystalline anisotropy can combine to yield two-patch tunneling in two ways. For example, simultaneous tunneling from two patches might occur for a single orientation. Superposition of two simple spectra, one for each patch, would then yield beats. Since simple spectra are commonly observed, at least one texture must be dominated by one-patch tunneling. If the second texture were to contribute two-patch tunneling, it would yield a beat-modulated spectrum by itself. One texture would then produce a simple spectrum, the other a beat modulated spectrum. Barring a degeneracy, this scenario generally requires *three* Fermi velocities, and tunneling must proceed entirely from just one or the other texture. Alternatively, the second texture may also contribute one-patch tunneling. Each texture is now dominated by a different patch, and beat modulated spectra require tunneling from suitable crystallites of both textures. This alternative requires only *two* Fermi velocities (v_{FS1}^* and v_{FS2}^*).

For either alternative, individual crystallies will contribute coherent level structure—over the entire bias range—only if they (a) are sufficiently clean ($l_S \approx d_S$), (b) extend all the way through the film and (c) are sufficiently smooth. Simple spectra presumably result when the junction area ($\approx 0.5 \times 0.5$ mm) contains only the dominant texture or, perhaps more likely, when the minority texture fails to satisfy (b) or (c).

We will adopt the simpler alternative that attributes one

dominant patch to each texture. Internal consistency then requires that (1) all beat modulated spectra yield the same two velocities, v^*_{FS1} and v^*_{FS2}, (2) all simple spectra yield the same velocity, v^*_{FS}, and (3) v^*_{FS} coincide with either v^*_{FS1} or v^*_{FS2}. The absence of simple spectra corresponding to v^*_{FS2} presumably means that minority-texture tunneling rarely occurs alone.

One might expect two velocities to imply two different energy gap values. As a practical matter, our junctions produce a single broadened gap signature. If there are two gaps, they probably differ by no more than 10% and are not resolved.

3. Organization

We will address several preliminary questions before proceeding to our main results. Specifically, we sill establish that (1) compound resonances cannot explain beat modulated spectra, (2) v^*_{FS1}, v^*_{FS2} and v^*_{FS} exhibit the anticipated internal consistencies, and (3) our λ values agree with other estimates. We will also examine the possibility that (4) a second, broadened energy gap produces a shoulder quantitatively resembling the DRBA. This agenda requires comparisons between computed spectra[6,11,12] and experiment. Because computed spectra depend on nominal estimates of $Z_S(E)$, we will often anticipate our results for $Z_S(E)$ in a self-consistent way. Again, our determinations of Fermi velocities and mass enhancements do not rely on this procedure.

B. Nonsimple spectra

1. Compound resonances

In the process of level formation, quasiparticle current incident on an In/Al interface from the indium side is either Andreev reflected, back into the In, or transmitted into the Al overlayer. These three currents are initially coherent. In the Wolfram limit ($l_N \ll d_N$),[6] the overlayer current is rendered incoherent by imperfection scattering and is therefore lost. Gallagher's theory is more general,[12] in that the overlayer current can be retained to produce additional interference effects. If the Al overlayer is sufficiently thick and clean ($l_N \approx d_N$), a beat-modulated In spectrum results.

Practical considerations do not favor a compound resonance explanation of our results. In their SQSE study of Al, Khim and Tomasch,[9] found that large mean-free-path values ($l_{Al} \geq 1$ μm) are quite difficult to achieve and require evaporation rates much larger than ours. Also, despite the stronger gap perturbations anticipated for Al/Pb bilayers (≤ 1.2 meV for Al/Pb versus ≤ 0.4 mV for In/Al), the Al level structure obtained in Ref. 9 (Al/Pb) is still quite weak. These considerations weigh against compound resonances in our In/Al bilayers. Nevertheless, such resonances can bear a disturbing qualitative resemblance to our beat-modulated spectra.

Although experimental microbalance estimates of d_N(Al) (≈ 0.2 μm) exist, we do not constrain d_N when parameterizing compound resonances. Success then depends on achieving agreement with experiment for plausibly small values of d_N and l_N. Our best compound-resonance fit to the experimental spectrum of Fig. 5 appears in Fig. 10. It reproduces the observed nodes at higher biases (curves *B* and *C* in Fig. 10) and yields the correct number of intervening levels. However, it also predicts a spurious node at lower bias (curve *A* in Fig. 10) and requires implausibly large values of d_N (0.85 μm) and l_N (5.5 μm).

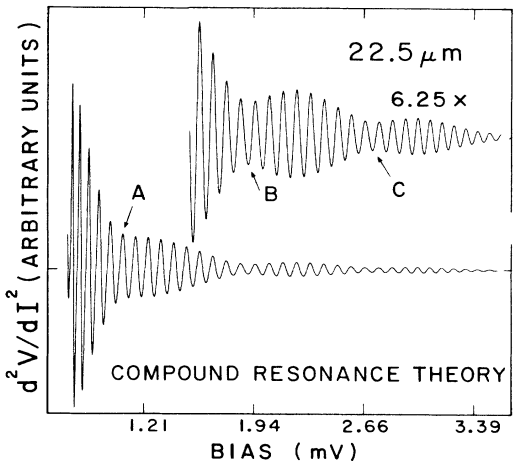

FIG. 10. Best compound-resonance fit to the d^2V/dI^2 spectrum of Fig. 5. Although this spectrum successfully reproduces the experimental high-bias nodes (*B* and *C*) and yields the correct number of oscillations (levels) between these nodes, it also predicts a spurious low-bias node (*A*).

The experimental second derivative spectrum presented in Figs. 11 and 12 is noteworthy for a low-lying beat node (arrow of Fig. 11) attributable to the large In thickness (41.0 μm). Our best compound-resonance fit (not shown) places the highest-energy beat node at about the

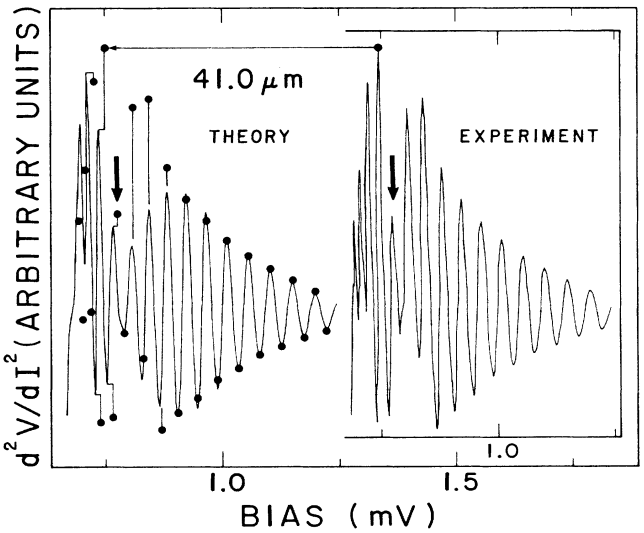

FIG. 11. Low-bias portion of a beat modulated experimental spectrum ($T = 0.9$ K) and a SGTV fit to this spectrum. Dots locate experimental peaks and dips. Theory successfully locates the lowest node (arrow) produced by this very thick In film.

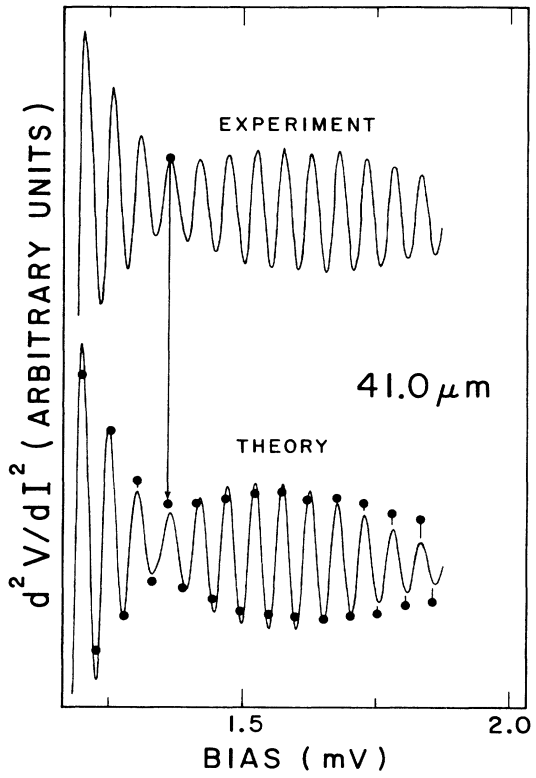

FIG. 12. High-bias continuation of Fig. 11. Good agreement extends to the highest biases (not shown).

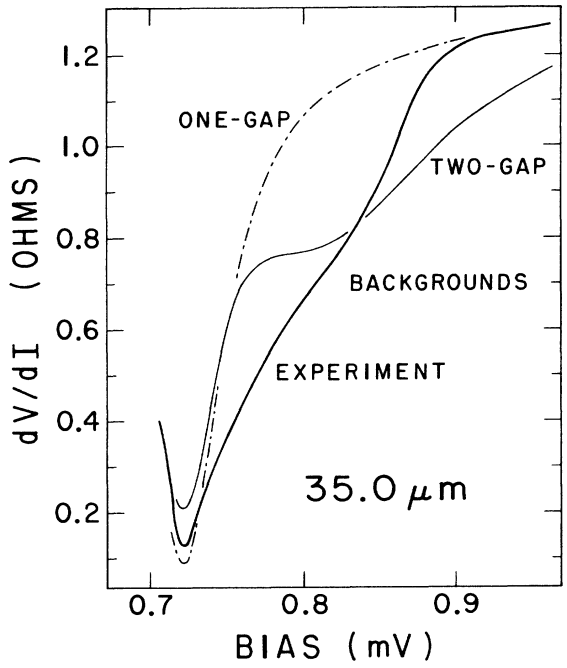

FIG. 13. Attempted simulation of the DRBA with a two-gap model. Oscillations are suppressed by setting assuming a short mean free path. Experimental and strong-coupling BCS backgrounds are taken from Fig. 9.

correct bias ($V \approx 2.2$ mV). However, the only other node predicted is too low in bias ($V \approx 1.2$ mV) and traps too many oscillations (18 versus 15) between nodes. Failure to reproduce the lowest-lying node (arrow of Fig. 11) is still more serious. Even this poor agreement with experiment requires a large d_N (1.5 μm) and an extremely large l_N (11.7 μm). We conclude that compound resonances do not provide a quantitatively successful alternative.

2. *Double-gap model for beats and the DRBA*

We have computed superpositions (admixtures) of two simple spectra, each with its own sharply defined gap value, to ascertain whether a sharp second gap could give rise to the DRBA shoulder. Our experience is that admixtures sufficient to yield beats also yield a second resolved SGS. Experimentally, only one signature is resolved. We therefore abandon this possibility.

An improved attempt to simulate a DRBA is summarized in Fig. 13. It utilizes a second gap whose SGS is smeared by the addition of an imaginary constant (10%) to the real gap. (For convenience, level structure is suppressed by use of a small mean free path.) Although an improvement over the first result, the DRBA shoulder is too pronounced at lower biases and too persistent at higher biases. It seems likely, however, that a distribution of sharper gaps could be designed to yield an acceptable shoulder.

3. *Single-gap, two-velocity (SGTV) model for beats*

The experimental spectra of Figs. 6, 7, 11, and 12 are accompanied by our best SGTV fits ($V \geq 1.0$ mV) computed for these spectra. All computed spectra already incorporate our results for $\mathrm{Re}Z_S(E)/Z_S(0)$ (Fig. 14) and utilize the complex variation of $\Delta_S(E)$ available from Rowell-McMillan tunneling spectroscopy.[14] Figures 6, 7, 11, and 12 typify the good agreement realizable at biases $V > 1.0$ mV. The lowest node of Fig. 11 is also reproduced.

Figure 15 includes a detailed comparison of all computed and observed level locations ($0.7 \leq eV \leq 3.5$ meV) for the dV/dI and d^2V/dI^2 spectra of Figs. 6 and 7. Agreement for dV/dI (two centermost lines labeled B) is excellent at all biases. Comparably good agreement is also realized for dV^2/dI^2 (lowermost two lines) at all biases. Continued good agreement at higher biases means that the $\mathrm{Re}Z_S(E)/Z_S(0)$ variation of Fig. 14, originally inferred from a simple spectrum (Fig. 2), accurately describes beat-modulated spectra.

Agreement with experiment depends sensitively on v^*_{FS1} and v^*_{FS2}. Sufficiently complete information exists for three beat-modulated spectra involving different In thicknesses. Detailed fits to these spectra yield just two, well-resolved velocities, $v^*_{FS1} = (1.166 \pm 0.014) \times 10^6$ (m/s) and $v^*_{FS2} = (1.062 \pm 0.015) \times 10^6$ (m/s).

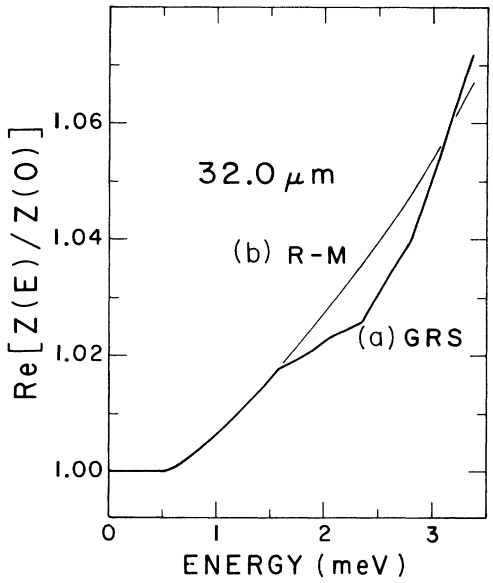

FIG. 14. Curve (a) is the SQSE variation for $\mathrm{Re}Z_S(E)/Z_S(0)$ obtained by fitting level locations for the representative dV/dI spectrum of Fig. 2. Curve (b) is the MRTS result (Ref. 14).

C. Simple spectra

1. v^*_{FS} from low-bias level spacings

Whereas extraction of v^*_{FS1} and v^*_{FS2} requires a parameterized fit over the entire energy (bias) range, extraction of v^*_{FS} from a simple spectrum requires knowing only d_S and the low-bias level spacing. At lower biases corresponding to $E_n \approx (eV_n - \Delta_{CE}) < 1.5$ meV, elementary arguments[4,5] show that $\Omega_S(n) = (E_n^2 - \Delta_S^2)^{0.5}$ versus n is essentially linear, where V_n locates the nth level (peak or dip) of dV/dI. Figure 16 shows that $\Omega_S(n)$ is quite linear and, hence, that v^*_{FS} is easily determined from the slope, $d\Omega_S/dn = hv^*_{FS}/2d_S$.

Sufficiently complete data exist for twelve junctions, and these yield $v^*_{FS} = (1.156 \pm 0.007) \times 10^6$ (m/s). This value overlaps $v^*_{FS1} = (1.166 \pm 0.014) \times 10^6$ (m/s) but not $v^*_{FS2} = (1.062 \pm 0.015) \times 10^6$ (m/s). This v^*_{FS} value also produces a good fit to the spectrum of Fig. 2.

2. Determination of $\mathrm{Re}Z_S(E)$

With increasing bias (energy), continued agreement for level locations (V_n) requires progressive increases in $\mathrm{Re}Z_S(E)$. Figure 15 presents the $\mathrm{Re}Z_S(E)/Z_S(0)$ obtained from empirical computer fits to the simple dV/dI spectrum of Fig. 2. As the upper two lines of Fig. 15 indicate, agreement for the dV/dI energy levels is quite good at all biases.[15]

Figure 14 [curve (b)] also presents $\mathrm{Re}Z_S(E)/Z_S(0)$ obtained from McMillan-Rowell tunneling spectroscopy (MRTS).[14] The two results are quite similar, although as we shall see, the two methods give rather different estimates of $Z_S(0)$.

3. SQSE estimates of mass enhancements

We now combine our v^*_{FS} and v^*_{FS2} values with theoretical bare velocities, v_{FS}, to estimate the mass enhancement $\lambda = (v_{FS}/v^*_{FS} - 1)$. For the second-zone hole (SZH) surface, Bhattacharyya and Swihart[16] give $v_F[001] = 1.71 \times 10^6$ (m/s) and $v_F[111] = 1.72 \times 10^6$ (m/s), which are quite similar to results by Hoff, de Groot, and Randles.[17] Clearly, band-structure calculations predict very little anisotropy in the bare-quasiparticle group velocity. There are several ways in

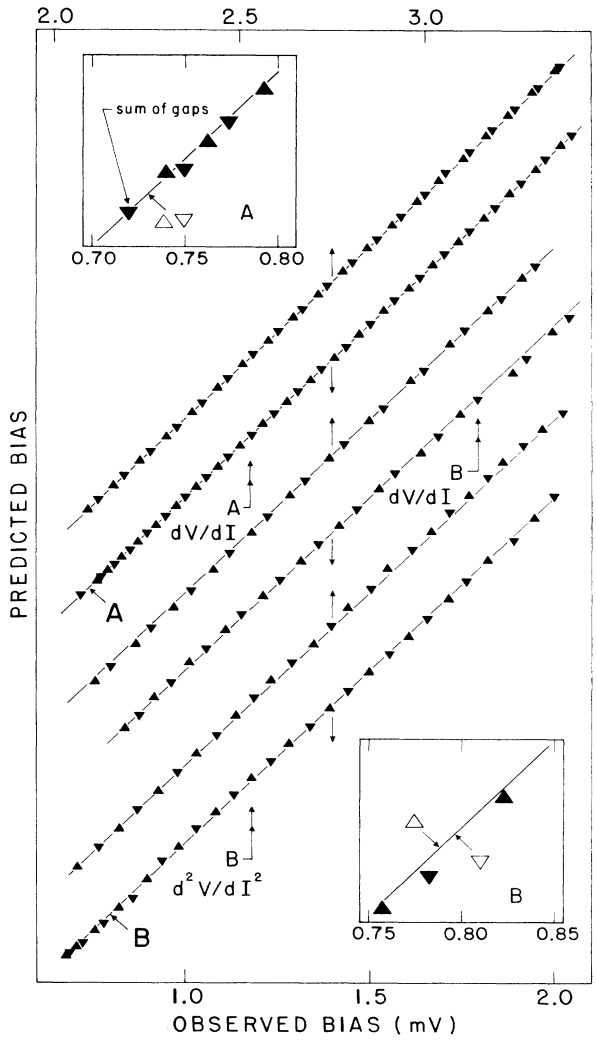

FIG. 15. Predicted and observed level locations plotted as ordinate (y) and abscissa (x), respectively. All computed results utilize the real renormalization variation of Fig. 15, designed to fit the simple dV/dI spectrum of Fig. 2. Arrows point to appropriate bias scales and straight lines ($y = x$) represent perfect agreement. A SGSV fit (labeled A) is used for the simple spectrum of Fig. 2, and a SGTV fit (labeled B) is used for the beat modulated spectrum of Fig. 6. Insets indicate minor disagreements very near the gap edge. For A (upper inset), the lowest level is not predicted, probably because of a very steep background slope. For B (lower inset), minor structure s missing in d^2V/dI^2.

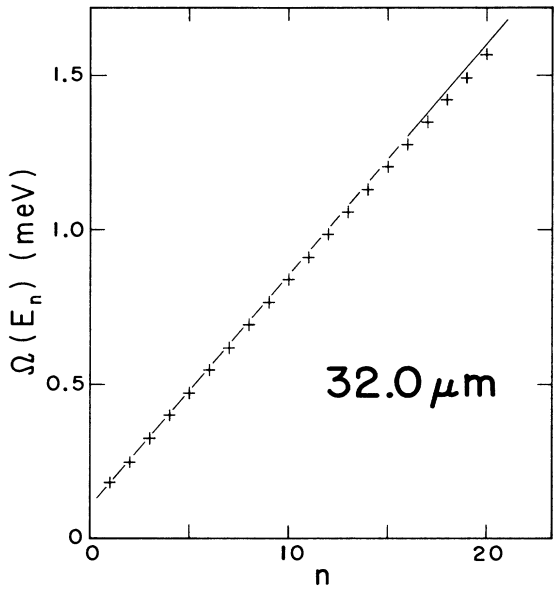

FIG. 16. $\Omega(E_n)$ vs n, where $\Omega(E_n)=[(eV_n-\Delta_{CE})^2-(\Delta_S)^2]^{0.5}$ and where $n=1,2,3,\ldots$ labels consecutive peaks and dips in dV/dI. The gap-edge value, $\Delta_S=0.534$ meV, is obtained from $I(V)$.

which our dressed velocities can be combined with the above.[16] These are presented in Table I along with λ (SZH) values predicted by Bhattacharyya and Swihart.[16,18] Agreement with Ref. 18 is best if simple spectra are attributed to [001] tunneling. This preference for [001] tunneling is in harmony with our x-ray results, which indicate a dominant [001] texture. Interpreted this way, v^*_{FS} and v^*_{FS2} yield $\lambda[001]=0.49$ and $\lambda[111]=0.62$, respectively. Agreement with theoretical SZH values[18] is reasonably good (Table I).

Predicted third-zone electron (TZE) velocities[16] are smaller than SZH values and, when combined with v^*_{FS} and v^*_{FS1}, yield λ values (0.09—0.41) much smaller than anticipated (0.71—0.79).[18] Hence SQSE velocities indicate that second-zone holes dominate [001] and [111] tunneling.

TABLE I. Experimental and theoretical estimates of $\lambda=[1-Z_S(0)]$ based on the second-zone hole surface of In. The first two rows comprise the preferred interpretation.

(v^*_{FS})[a]	$[hkl]$[b]	λ(SQSE)	λ(theory)[c]	$\delta\lambda$[d]
1.15[e]	[001]	0.49	0.51	−4%
1.06[f]	[111]	0.62	0.57	+ 8%
1.15	[111]	0.50	0.57	−14%
1.06	[111]	0.62	0.57	+ 8%
1.15	[001]	0.49	0.51	−4%
1.06	[001]	0.61	0.51	+ 16%
1.15	[111]	0.50	0.57	−14%
1.06	[001]	0.61	0.51	+ 16%

[a]Units are 10^6(m/s).
[b]Direction attributed to v^*_{FS}.
[c]See Ref. 18.
[d]Difference between experiment and theory.
[e]Experimental (SQSE) value of v^*_{FS}.
[f]Experimental (SQSE) value of v^*_{FS2}.

Surprisingly, the MRTS (Ref. 14) λ value (0.79) is more appropriate for TZE tunneling (0.71—0.79) than for SZH tunneling (0.51—0.73).[18,19] Although of unspecified thickness, the MRTS film was probably much thinner than any of our In films. Randomly oriented crystallites could cause TZE tunneling to dominate and might explain the MRTS result. Clearly, crystalline tecture is an important sample parameter for both spectroscopies.

4. *Determination of* $\mathrm{Im}Z_S(E)$

Just as $\mathrm{Re}Z_S(E)/Z_S(0)$ can be varied to adjust computed level locations, $\mathrm{Im}Z_S(E)$ can be varied to adjust computed amplitudes as a function of energy (bias). Our experimental spectra do not, however, lend themselves to a simple amplitude analysis—a fact attributable to the LBAA. We have constrained our attempts to fit observed amplitudes by requiring $\mathrm{Im}Z_S$ ($E\leq 1.5$ meV) and α^2F ($\omega\leq 1.5$ meV) to behave simply, remain positive, and approach zero as E and ω approach zero. These modest requirements significantly limit the agreement attainable. Our best fit is a compromise that underestimates amplitudes in the upper DRBA/LBAA range and *overestimates* amplitudes in the lower DRBA/LBAA range (as in Fig. 3). Furthermore, even this limited success requires a variation of $\mathrm{Im}Z_S(E)$ that may well be artificial.

Although defect scattering sets the overall amplitude scale (via γ_S), increases in $\mathrm{Im}Z_S(E)$ provide the progressive phonon emission required with increasing energy. Since $\mathrm{Im}Z_S(E)$ is expected to approach zero for small energies, we adjust γ_S to fit amplitudes at low biases. As will become clear, the LBAA may well impair the utility of this approach. Curve (a) of Fig. 17 presents an estimate of $\mathrm{Im}Z_S(E)$ based on a γ_S that is appropriate for amplitudes in the upper DRBA/LBAA range. [Note: curve (a) of Fig. 17 is *likely to be unreliable* below $E\geq 3.0$ meV.] Curve (a) already embodies the constraints mentioned above.

Defects in the amplitude fits produced by this $\mathrm{Im}Z_S(E)$ can be seen in Fig. 3 ($eV<0.9$ meV), where the first three computed oscillations are overestimated. Figure 18 provides a detailed amplitude comparison for the spectrum of Fig. 2 by plotting amplitude ratios (theory/experiment) as a function of bias.[20] Above $V\geq 1.0$ mV, departures from perfect agreement (horizontal line) do not exceed 5%. In the upper DRBA/LBAA range (0.85—0.95 meV), amplitudes are underestimated by as much as 18%. In the lower DRBA/LBAA range, they are *overestimated* by as much as 48%.

Structure in Fig. 17(a)—a peak near 1.2 meV and a dip near 2.5 meV—occurs at biases well above the DRBA/LBAA range. Attempts to associate these features with vestigial nodes and antinodes (SGTV model) invariably fail because additional, unobserved beats are predicted. We will argue that this structure in $\mathrm{Im}Z_S(E)$ is probably an artifact produced by the impact of the LBAA on the fitting process.

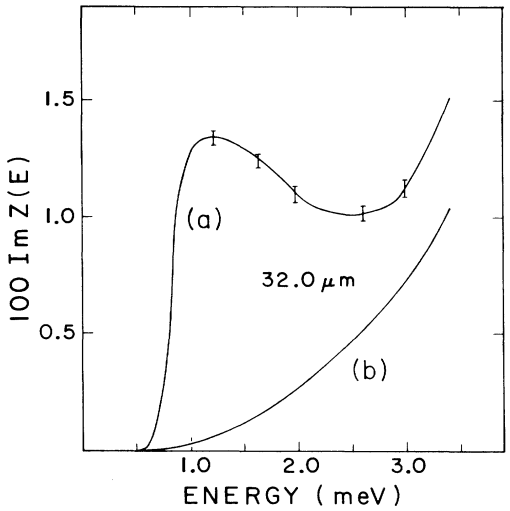

FIG. 17. The SQSE variation of $\mathrm{Im}Z_S(E)$, obtained by fitting amplitudes of Fig. 2 subject to reasonable constraints on $\alpha^2F(\omega<0.5$ meV), appears as curve (a). Its unusual character ($E<3.0$ meV) is probably an artifact produced by the LBAA. Curve (b) is a more conventional variation that does not attempt to reproduce amplitudes in the LBAA range. At lower biases, curve (a) produces a compromise that underestimates amplitudes in the upper LBAA range and *overestimates* amplitudes in the lower LBAA range, as in Fig. 3. Curve (b) seriously underestimates amplitudes over the entire LBAA range, as in Fig. 6.

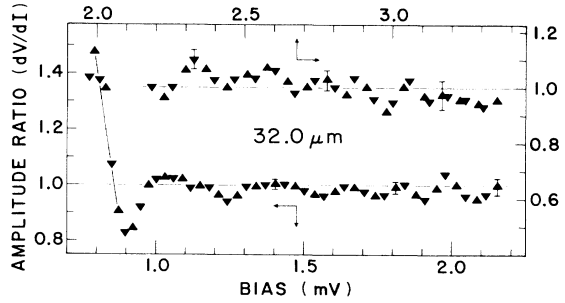

FIG. 18. Amplitude ratios (theory/experiment) for the dV/dI spectrum of Fig. 2. Use of curve (a) (Fig. 17) for $\mathrm{Im}Z_S(E)$ produces a compromise in which amplitudes in the upper LBAA range are underestimated ($\lesssim 18\%$) and amplitudes in the lower LBAA range are overestimated ($\lesssim 48\%$). Use of curve (b) (Fig. 17) substantially underestimates amplitudes over the entire LBAA range.

Since amplitudes vary approximately as $\exp[-\gamma_S - \pi C_S\,\mathrm{Im}Z_S(E)E]$, γ_S is fit to low-bias amplitudes, where the influence of $\mathrm{Im}Z_S(E)$ is supposedly negligible. Because of the LBAA, however, this may underestimate γ_S by a constant amount $(-|\delta\gamma_S|)$. Maintenance of agreement for amplitudes above the LBAA bias range then requires a compensating overestimate of $\mathrm{Im}Z_S(E)$—by an amount $\delta[\mathrm{Im}Z_S(E)]\approx|\delta\gamma_S|/\pi C_S E$. Consequently, $\mathrm{Im}Z_S(E)$ acquires a spurious energy dependence to compensate for $-|\delta\gamma_S|$.

Since $\delta[\mathrm{Im}Z_S(E)]$ diminishes as $1/E$ and since phonon damping increases rapidly near E_S, $\delta[\mathrm{Im}Z_S(E)]$ would be least important at higher energies. Indeed, the $\mathrm{Im}Z_S(E)$ of Fig. 17 reverts to a steadily rising function above $E\geq 3.0$ mV. The peak and dip of Fig. 17 may, therefore, represent effects of an artificial $1/E$ dependence that is truncated at low energies ($E<1.0$ meV) by imposition of constraints. If so, curve (a) (Fig. 17) should approach the true variation at the highest energies. Curve (b) (Fig. 17) represent an attempt to correct for this defect and probably represents a more reasonable estimate of $\mathrm{Im}Z_S(E)$.

If multiplied by ten, curve (b) (Fig. 17) approximates the MRTS result for $\mathrm{Im}Z_S(E)$.[14] Even above $E\geq 3.0$ mV, values by MRTS are six to ten times larger than by SQES. Employing the MRTS result for $\mathrm{Im}Z_S(E)$, computed spectra exhibit level quenching by $E_S=2.1$ meV instead of by the observed $E_S=3.5$ meV. The MRTS result is therefore too large for either [001] or [111] tunneling. Because of decreased sensitivity at lower energies, MRTS necessarily relies on extrapolations of $\alpha^2F(\omega)$ to estimate $\mathrm{Im}Z_S(E)$. Attendant uncertainties may explain the difference between the MRTS and SQSE results. Alternatively, the MRTS result could be due to differences in crystalline orientation. But if so, α^2F ($\omega<3.5$ meV) is much more anisotropic than λ, i.e., than $\alpha^2F(\omega)/\omega$ integrated over energy.

Numerical inversion of the appropriate Eliashberg equation,

$$\mathrm{Im}Z(E)=(\pi/E)\int_0^E d\omega\alpha^2F(\omega)\,\mathrm{Re}[1-\Delta^2(E-\omega)/(E-\omega)^2]^{-1/2}\,, \tag{1}$$

permits one to infer $\alpha^2F(\omega)$ from $\mathrm{Im}Z_S(E)$. Figure 19 presents the $\alpha^2F(\omega)$ appropriate for the $\mathrm{Im}Z_S(E)$ of Fig. 17(a). As anticipated, our results are much smaller than those from MRTS, even for above $\omega\geq 3.0$ mV. The peak and dip of Fig. 19 reflect similar behavior in $\mathrm{Im}Z_S(E)$ and may, therefore, be artifacts. But if so, the $\alpha^2F(\omega)$ of Fig. 19 should approach the actual variation at higher phonon energies, say above 2.5 meV.

IV. SUMMARY AND DISCUSSION

A. Summary of experimental results

For twelve junctions which produce simple spectra and for which sufficiently complete data exist, we infer one well-defined Fermi velocity, $v_{FS}^{*}=(1.156\pm0.007)\times10^6$ (m/s). For three junctions which produce beat-modulated

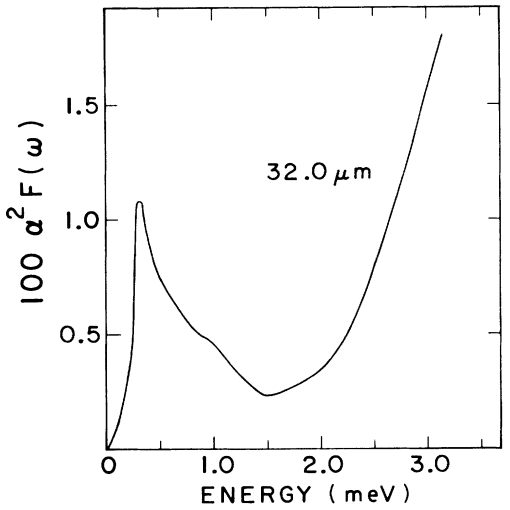

FIG. 19. The $\alpha^2F(\omega)$ variation appropriate for curve (a) of Fig. 16. The peak near 0.5 meV is probably an artifact produced by the low-bias amplitude anomaly.

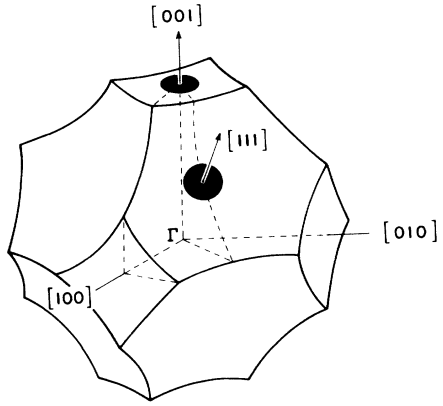

FIG. 20. Second-zone hole (SZH) surface for In. Dark patches are expected to contribute tunneling for the [001] and [111] textures.

spectra and for which sufficiently complete data exist, we infer two well-resolved velocities, $v^*_{FS1}=(1.166\pm0.014)\times10^6$ (m/s) and $v^*_{FS2}=(1.062\pm0.015)\times10^6$ (m/s). The small spread in v^*_{FS} and the close agreement between v^*_{FS} and v^*_{FS1} suggest that one specific patch on the Fermi surface always contributes to tunneling and, by itself, yields simple spectra. The small spread in $v^*_{FS2}(\approx1.5\%)$ suggests that a second specific patch sometimes contributes to tunneling and thereby yields beat-modulated spectra. Binary crystalline textures exhibited by our In films are the likely source of this behavior.

Our estimates of mass enhancements—$\lambda[001]=0.49$ (from v^*_{FS}) and $\lambda[111]=0.62$ (from v^*_{FS2})—are appropriate for second-zone hole (SZH) tunneling (Table I). Unreasonably small mass enhancements result if third-zone electron (TZE) tunneling is assumed to dominate. Whereas beat-modulated spectra yield two well-resolved velocities ($\approx8\%$), they do not exhibit two resolved gaps. Instead, the sum-of-gaps signature may be smeared by a comparable amount. Our measurements also yield an average gap value of $\Delta_S=(0.53\pm0.01)$ meV. When combined with v^*_{FS}, this yields a nominal coherence length $\xi_{BCS}=0.23\ \mu$m.

Except for minor differences, $\mathrm{Re}Z_S(E)/Z_S(0)$ obtained by SQSE [curve (a), Fig. 14] is quite similar to that by McMillan-Rowell tunneling spectroscopy (MRTS).[14] However, MRTS yields a λ value (0.79) more appropriate for third-zone electron tunneling.[18,19] MRTS estimates of $\mathrm{Im}Z_S(E)$ are also too large for the smaller phonon damping ($E_S=3.6$ meV) that we observe for [001] or [111] tunneling. Either MRTS overestimates $\mathrm{Im}Z_S$ ($E\lesssim3.6$ meV) and α^2F ($\omega\lesssim3.6$ meV), or these quantities are substantially more anisotropic than λ, i.e., than $\alpha^2F(\omega)/\omega$ integrated over energy.

Strong dV/dI spectra exhibit a dynamic-resistance background anomaly (DRBA). This consists of a shoulder approximately 0.2 mV wide, located about 0.1 mV above the sum-of-gaps signature. Its occurrence apparently requires high-quality In crystallites capable of producing strong SQSE structure. Simple, beat-modulated, and complex spectra all exhibit the DRBA.

Strong spectra also exhibit a low-bias amplitude anomaly (LBAA), in which level amplitudes are too large compared to those at intermediate and higher biases. The DRBA and LBAA occupy the same bias range and may or may not be directly related.

B. Fermi surface considerations

Figure 20 depicts the In SZH surface.[18,19] It is nearly free-hole-like along the [001] and [111] directions, with v^*_F parallel to k_F. The [111] patch contributes to tunneling only near [111], and the [001] patch contributes only near [001].[21] Figure 21 presents the TZE surface, whose β arms can contribute along both directions.[21,22] Our λ values indicate that SZH tunneling dominates, and SZH

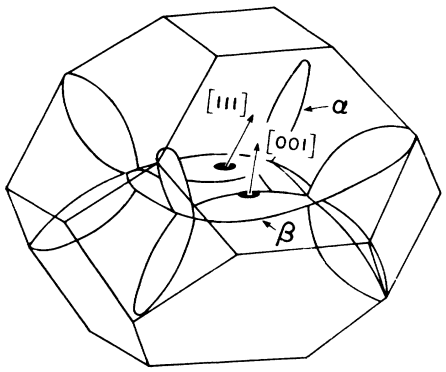

FIG. 21. Third-zone electron (TZE) surface. Dark patches on the α arms and β arms are expected to contribute tunneling for the [001] and [111] textures. The effective areas of these patches may be much smaller than those of Fig. 20.

topology suggests that v^*_{FS} and v^*_{FS2} represent tunneling from the majority [001] and minority [111] textures, respectively. In the simplest view, [001] patches produce simple spectra, and [001] and [111] patches, together, produce beat modulated spectra.

This interpretation requires a negligible TZE contribution to level formation, even though β-arm tunneling is permitted for both textures. Since tunneling matrix elements decrease rapidly with tunneling angle, high β-arm curvatures may well restrict TZE tunneling to very small patches (Fig. 21). It seems unlikely that TZE tunneling can play a general role in beats, otherwise all spectra should exhibit beats.

C. The DRBA

Even if TZE tunneling is too weak to influence level amplitudes, it may still explain the DRBA. A sum-of-gaps signature (SGS) comprises extremely strong structure, and hence even minor TZE tunneling could produce a weak SGS identifiable with the DRBA. Our attempts to simulate a DRBA with a second gap suggest weak tunneling and a distribution of gap values. Interpreted this way, the DRBA of Fig. 8 (inset) yields an average gap $\Delta_S(\mathrm{TZE}) \approx 0.65$ meV. In two instances, we observe complex spectra after long anneals at room temperature. TZE tunneling may also play a role here, since it could provide a natural explanation for the small level spacings that reoccur in the DRBA range. These spacings would mark initiation of a new series at $eV=[\Delta_{CE}+\Delta_S(\mathrm{TZE})] \approx 0.8$ meV (Fig. 9), the larger $\Delta_S(\mathrm{TZE})$ being appropriate for the larger $\lambda(\mathrm{TZE})$ (0.71—0.79). Annealing may serve to produce an occasional crystallite with a low-symmetry orientation, so that TZE tunneling dominates. This view suggests that complex spectra may also exhibit an enhanced DRBA. Our limited experience is compatible with this view. TZE tunneling requires high-quality In, which could explain the apparent correlation between the DRBA and strong amplitudes. From this view, the LBAA and the DRBA are not directly related.

D. The LBAA

It seems unlikely that TZE tunneling would give rise to the observed LBAA—a simple amplitude anomaly, confined to lower biases and devoid of spacing irregularities. Instead, one might expect TZE tunneling to yield effects more like those of complex spectra. Furthermore, arguments against the LBAA being caused by residual beats or compound resonances are compelling. Two conceivable alternatives are given below. One invokes surface roughness, the other gap enhancement.

1. Surface roughness

The SQSE results of Wong, Shih, and Tomasch[10] for Zn/Pb display behavior that could be relevant. In addition to producing bound states ($eV \leq \Delta_{Pb}$), such bilayers also produce virtual states at higher biases. Three of their eight bilayers produce virtual states whose amplitudes decay with anomalous rapidity at higher biases. Although these three yield bound states as strong as the others and yield the same v^*_{FN} (Zn) value as the others, their virtual states are quenched at substantially lower biases. If one were to place normally and anomalously behaved Zn/Pb bilayers in parallel, one would obtain a composite tunneling spectrum in which virtual states at higher biases appear too weak but, nevertheless, persist to high biases. It is conceivable that the anomalously rapid decline of Zn/Pb amplitudes is related to surface roughness.

Virtual-state levels are associated with quasiparticle standing waves whose wavelengths decrease with increasing energy (bias). Film roughness therefore becomes increasingly important with increasing bias. To the extent that an actual film behaves like a distribution of In thicknesses, one expects destructive interference to progressively weaken amplitudes with increasing bias. Since bound states have no role at higher biases, this picture could apply equally well to Zn/Pb and In/Al.

For this interpretation, most In crystallites (1) are smooth, (2) have the measured thickness, and (3) produce virtual levels that are phonon quenched at a high bias ($E_S=3.5$ meV). The remaining crystallites can be rough, or they can smooth with a distribution of thicknesses. Either way requires a roughness that remains approximately constant at 15%, independent of In thickness, so that the LBAA can appear to be a universal property. Such constancy, for so may bilayers and for so wide a range of thicknesses ($d_S=5$—41 μM), would be surprising. As a result, this type of explanation strikes us as contrived.

2. Gap enhancement

Although controversial, a simple ansatz that accounts for enhanced level amplitudes is an enhanced gap perturbation $[\delta\Delta \approx (\Delta_{In}-\Delta_{Al}) \approx \Delta_{In}]$. Since Andreev scattering goes as $\delta\Delta$, increased scattering can yield stronger level structure. In general, the effective In gap could increase in either of two ways. It could (a) undergo a spatially uniform enhancement that is localized in energy, just above the gap edge; or it could (b) undergo a spatially localized increase near the interface, leading to quasibound levels. Both can yield enhanced amplitudes in the LBAA range. Alternative (a) would imply a peak in $\mathrm{Re}\Delta_S(E)$, located about 0.1 meV above the gap edge, and would imply a bulk effect. Alternative (b) would imply an interfacial effect.

a. *Energy-local enhancement.* Assuming the usual strongcoupling picture, a spatially uniform gap enhancement naturally yields correlations between the LBAA and the DRBA. The required peak in $\mathrm{Re}\Delta_S(E)$ causes a corresponding peak in the background density of states, $N_S(E) \approx E/[E^2-\Delta_S^2(E)]^{0.5}$. This in turn produces a DRBA-like dip (shoulder) in dV/dI. A moderate peak ($\approx 10\%$) in $\mathrm{Re}\Delta_S(E)$ would roughly account for both anomalies. It would presumably imply a correspondingly peak in $\alpha^2F(\omega)$, a peak of unspecified physical origin.

b. *Spatially local enhancement.* A spatially localized gap that exceeds both component gap values would seem to require (1) a favorable change in electron-phonon interaction near the interface or (2) a metallurgical reaction at the interface. Neither way of realizing spatially localized gap enhancements suggests correlations between the LBAA and the DRBA.

According to estimates by Menon and Arnold,[23] interfacial electron-phonon effects are too small to make alternative (1) likely. According to the bulk phase diagram, In and Al are immiscible and form no compounds. It is conceivable, however, that In/Al reacts to produce an interfacial (nonbulk) superconductive phase. The formation of an interfacial phase has been recently reported for In/Cu.[24]

Future proximity effect tunneling experiments on Al overlayers (In/Al-Al oxide-Al) may be able to detect gap enhancements, if they actually occur.

E. Final remarks

The LBAA clouds the meaning of $\mathrm{Im}Z_S(E)$ and $\alpha^2F(\omega)$ determined by SQSE at energies below 3.0 meV. Based on existing information, surface roughness remains a possible, if improbable, alternative for the LBAA. Scenarios based on gap enhancement are controversial, but can be tested by future tunneling experiments. At this juncture, both the LBAA and the DRBA are of uncertain origin.

ACKNOWLEDGMENTS

We are indebted to J. C. Swihart for helpful discussions and for providing SZH and TZE group velocities. We gratefully acknowledge Mr. C. A. Gaffney for additional compound resonance calculations. We also acknowledge helpful conversations with G. B. Arnold. This work was supported in part by the National Science Foundation under Grant No. DMR 81-05007-04.

---

*Current address: Boeing Aircraft Corporation, Wichita, Kansas.

†Current address: Department of Physics, Chung-Yuan Christian University, Chung-Li, Taiwan, Republic of China.

[1]A. F. Andreev, Zh. Eksp. Teor. Fiz. **46**, 1823 (1964) [Sov. Phys.—JETP **19**, 1228 (1964)].

[2]W. J. Tomasch, Phys. Rev. Lett. **15**, 672 (1965).

[3]W. J. Tomasch, Phys. Rev. Lett. **16**, (1966).

[4]W. L. McMillan and P. W. Anderson, Phys. Rev. Lett. **16**, 85 (1966).

[5]W. J. Tomasch and T. Wolfram, Phys. Rev. Lett. **16**, 352 (1966).

[6]T. Wolfram, Phys. Rev. **176**, 482 (1968).

[7]G. I. Lykken, A. L. Geiger, K. S. Dy, and E. N. Mitchell, Phys. Rev. B **4**, 1523 (1971).

[8]S. L. Colucci, W. J. Tomasch, and Hyung Joon Lee, Phys. Rev. Lett. **32**, 590 (1974).

[9]Z. G. Khim and W. J. Tomasch, Phys. Rev. B **18**, 4706 (1978).

[10]L. S. Wong, S. Shih, and W. J. Tomasch, Phys. Rev. B **23**, 5775 (1981).

[11]G. B. Arnold, Phys. Rev. B **18**, 1076 (1978).

[12]W. J. Gallagher, Phys. Rev. B **22**, 1233 (1980).

[13]The DRBA is not as easily detected in strong spectra of thinner In films ($\lesssim 25$ μm) because fewer oscillations occur within the DRBA range, providing fewer nodes to trace out the DRBA. Under these circumstances, anomalies remain detectable via characteristic lineshape distortions (arrows in Fig. 8) caused by a rapidly changing dV/dI background.

[14]J. M. Rowell, W. L. McMillan, and R. C. Dynes, (unpublished).

[15]Owing to the rapidly changing background just above the gap edge, the first computed level is difficult to resolve for practical grid sizes. This situation is depicted in the upper inset of Fig. 15.

[16]B. K. Bhattacharyya and J. C. Swihart (private communication).

[17]A. B. M. Hoff, D. G. de Groot, and D. L. Randles, J. Phys. F **6**, L141 (1976).

[18]B. K. Bhattacharyya and J. C. Swihart, J. Phys. F **14**, 1651 (1984).

[19]N. W. Ashcroft and W. E. Lawrence, Phys. Rev. **176**, 938 (1968).

[20]Our computed level amplitudes are insensitive to decreases in computational grid size. Also, compound resonances cannot be invoked to explain the LBAA, since such resonances actually decreases amplitudes in the LBAA range.

[21]We make the usual assumption that the tunneling selection rule is on the group velocity rather than on the crystal momentum.

[22]No α-arm tunneling is anticipated along the texture directions.

[23]Madhu Menon and Gerald B. Arnold, Phys. Rev. B **27**, 5508 (1983).

[24]W. Keppner, T. Klas, W. Korner, R. Wesche, and G. Schatz, Phys. Rev. Lett. **54**, 2371 (1985).